Journal of Carbon Research

MDPI

Article

Plasma-Enhanced Carbon Nanotube Fiber Cathode for Li-S Batteries

Yanbo Fang [1], Yu-Yun Hsieh [1], Mahnoosh Khosravifar [1], Paa Kwasi Adusei [1], Sathya Narayan Kanakaraj [1], Bely Stockman [2], Vamsi Krishna Reddy Kondapalli [1] and Vesselin Shanov [1,2,*]

[1] Department of Mechanical and Materials Engineering, University of Cincinnati, Cincinnati, OH 45221-0072, USA; fangyb@mail.uc.edu (Y.F.); hsiehyu@mail.uc.edu (Y.-Y.H.); khosramh@mail.uc.edu (M.K.); aduseipi@mail.uc.edu (P.K.A.); kanakasa@mail.uc.edu (S.N.K.); kondapvy@mail.uc.edu (V.K.R.K.)

[2] Department of Chemical and Environmental Engineering, University of Cincinnati, Cincinnati, OH 45221-0012, USA; stockmby@mail.uc.edu

* Correspondence: shanovvn@ucmail.uc.edu

Abstract: Fiber-shaped batteries have attracted much interest in the last few years. However, a major challenge for this type of battery is their relatively low energy density. Here, we present a freestanding, flexible CNT fiber with high electrical conductivity and applied oxygen plasma-functionalization, which was successfully employed to serve as an effective cathode for Li-S batteries. The electrochemical results obtained from the conducted battery tests showed a decent rate capability and cyclic stability. The cathode delivered a capacity of 1019 mAh g^{-1} at 0.1 C. It accommodated a high sulfur loading of 73% and maintained 47% of the initial capacity after 300 cycles. The demonstrated performance of the fiber cathode provides new insights for the designing and fabrication of high energy density fiber-shaped batteries.

Keywords: lithium-sulfur batteries; fiber battery; CNT; oxygen plasma functionalization; polysulfide

Citation: Fang, Y.; Hsieh, Y.-Y.; Khosravifar, M.; Adusei, P.K.; Kanakaraj, S.N.; Stockman, B.; Kondapalli, V.K.R.; Shanov, V. Plasma-Enhanced Carbon Nanotube Fiber Cathode for Li-S Batteries. *C* **2022**, *8*, 30. https://doi.org/10.3390/c8020030

Academic Editor: Jandro L. Abot

Received: 12 April 2022
Accepted: 20 May 2022
Published: 22 May 2022

1. Introduction

Recently, there has been an increasing interest in the development of flexible and wearable power sources due to the rise of wearable electronic devices, health monitoring, and epidermal sensors [1–3]. However, the flexibility of energy storage and conversion devices is limited by the electrodes, metal current collectors, and other rigid materials used [4]. The conventional fabrication of electrodes, using slurry casting on a metal current collector, lowers the mass loading of active materials and suffers from delamination, resulting in low energy density and poor cyclic ability [5]. Therefore, freestanding carbon materials such as graphene, carbon nanotube (CNT) sheets, and 3D graphene foam [6–9] are emerging as popular electrodes due to their flexibility and good electrical conductivity. Yet, because of the planar structure of these carbon electrodes, only limited bending directions are allowed, while they are still delicate when exposed to complex deformation in real-life handling. To overcome the geometrical restrictions of planar devices, 1D fiber-shaped devices have been proposed and attracted much attention [10–13]. These new generation energy storage devices exhibit unique advantages due to their excellent flexibility and the ability to be integrated with fabric, making them applicable as the power sources for wearable electronics.

Currently, traditional Li-ion batteries suffer from low energy density as they approach the theoretical limit of the active materials [14]. Lithium-sulfur (Li-S) batteries have become a promising candidate due to their high theoretical specific capacity of 1675 mAh g^{-1} and energy density of 2500 Wh kg^{-1} [15–18]. However, the development of Li-S batteries in a practical application has been hindered by poor cyclic performance, low Coulombic efficiency, and ineffective utilization of the active materials. One critical issue for Li-S

batteries is the low utilization of the active materials because of the low conductivity of sulfur, polysulfide shuttling effect, and the formation of insoluble and insulating lithium sulfides, Li_2S_2/Li_2S (LiS) on the cathode surface [19]. Carbon materials with excellent flexibility and electrical conductivity have been employed in the sulfur composite cathode to address this issue [17,20–31]. Despite the many efforts that have been devoted to developing fiber-shaped lithium-ion batteries and supercapacitors [32–35], only a few attempts have been made to create fiber-shaped Li-S batteries [36,37]. These efforts explored CNT composite materials to load sulfur for fiber-shaped Li-S batteries. Because they improve the utilization of sulfur and mitigate the polysulfide shuttling, these batteries exhibit stable cyclic ability. However, such strategies require a tedious process for synthesizing CNT composite, which also lowers the energy density due to the extra weight of the host materials. Conventional fabrication of cathodes for Li-S batteries requires pressing the slurry onto a metal current collector which involves active materials, binders, and conductive additives. Such a mixture unfavorably differentiates the mechanical property of the electrode in the different areas [27,38]. This limitation restricts their application in fiber-shaped batteries where the electrode will experience complex deformation. Our previous work has determined high porosity (~46%), decent electrical conductivity (~53 S cm^{-1}), and good mechanical robustness with excellent flexibility of CNT fiber [39]. All these qualities make it a promising material for the fiber cathode. One of the critical issues for the sulfur cathode is the low utilization of sulfur active material due to its low electrical conductivity [40,41]. Our previous study successfully alleviated this situation by oxygen plasma functionalizing 3D graphene [20]. The plasma functionalization conducted on 3D graphene altered its surface chemistry and enhanced the distribution of sulfur. As a result, refined sulfur particles were obtained which improved the utilization of the sulfur active material. We concluded that these effects were attributed to the oxygen functional groups that were created by plasma treatment on 3D graphene [20]. The same functional groups were also found in CNT fibers after oxygen plasma functionalization which was proven by XPS in our previous publication [42]. This suggests a likely similar enhancement for CNT sulfur cathodes by oxygen plasma treatment, as proved here.

In this work, we report a CNT fiber, enhanced by a facile oxygen plasma functionalization, as an effective host material for the sulfur cathode. The resulting fiber is a freestanding, flexible, and highly conductive material with implanted oxygen functional groups to accommodate and refine sulfur particles. These functional groups altered the surface of CNT, thus becoming hydrophilic and suitable for sulfur infiltrating. The porous host material also increases the sulfur loading, housing more than 70% of the sulfur. Eventually, these unique features improve the utilization of sulfur and suppress the polysulfide diffusion, enabling an excellent rate of cyclability and long cyclic stability in the test cells.

2. Materials and Methods

2.1. CNT Fiber Spinning and Oxygen Functionalization

Vertically aligned carbon nanotube arrays were synthesized in a modified commercial CVD reactor ET3000 from CVD Equipment Corporation. Oxidized single crystal silicon with aluminum oxide as a buffer layer and Fe-Co catalyst film on top was used as a substrate in the CVD process. The growth process parameters and the properties of the resulting array have already been published in our previous work [41]. A CNT ribbon was drawn from the end of the array and a continuous fiber was spun using a homemade spinning apparatus [42]. The "as-obtained" pristine CNT fiber is designated here as CNT fiber. The latter was then passed through a tubular plasma source (SurFx AtomFlo model 400-V2.0HE) operating at atmospheric pressure with the parameters: 100W power, 0.3 L/min flow of oxygen, and 15 L/min flow of helium. The functionalized fiber is assigned here as oxygen functionalized CNT (OCNT).

2.2. Fabrication of CNT-Sulfur (CNT-S) and Oxygen Functionalized CNT-Sulfur (OCNT-S) Composites

Both CNT-S and OCNT-S composites were prepared by a dry melting method. In brief, 20 cm of pristine or oxygen functionalized CNT fiber was coiled on a stainless-steel bobbin and was sealed in a 50 mL Teflon-lined stainless-steel autoclave filled with argon, together with 10 mg of sulfur. The autoclave was then heated at 156 °C for 12 h for sulfur to diffuse into the CNT fiber.

2.3. Materials Characterization

The morphology of the obtained materials was observed by scanning electron microscopy (SEM) (Philips FEI XL30, Eindhoven, Netherlands, 5–10 kV). Raman spectroscopy (Renishaw inVia, West Dundee, IL, USA) excited by a 514 nm Ar-ion laser with a laser spot size of ~1 μm^2 was used to characterize the OCNT and OCNT-S. Thermogravimetric analysis (TGA) (Q50, TA instrument, New Castle, DE, USA) was performed in a nitrogen atmosphere from room temperature to 600 °C at a heating rate of 10 °C min^{-1}. A Sartorius micro-analytical balance model ME5 with microgram resolution was utilized to precisely measure the mass of the CNT fibers and related composites.

2.4. Electrochemical Performance Measurements

OCNT-S and CNT-S fiber electrodes were evaluated in a coin cell setup with lithium foil as the counter and reference electrodes. In total, 10 cm of the fibers was cut and coiled into a pellet and used as a cathode without adding any conductive additives or binders. The sulfur loading determined by the TGA analysis was ~70%. All electrochemical tests were carried out in an electrolyte which was a mixture of 1 M lithium bis-trifluoromethanesulfonylimide in 1,3-dioxolane and 1,2-dimethoxyethane (1:1 by volume) with 1 wt% $LiNO_3$ additive. The volume of electrolyte was 20 µL in all assembled cells. A polypropylene film (Celgard 2400) was used as a separator in the cell. A galvanostatic charge–discharge instrument (LANHE CT2001A, Wuhan, China) was employed to characterize the performance of the battery coin cell. The Li-S batteries were galvanostatically charge/discharge cycled between 1.5 and 2.8 V at 0.1 C to 2 C (1 C = 1675 mA g^{-1}). The electrochemical impedance spectroscopy (EIS) of the cells were conducted using a Potentiostat (Gamry Interface 1000E, Warminster, PA, USA).

3. Results and Discussion

The SEM images of CNT-sulfur (CNT-S) and oxygen functionalized CNT-sulfur (OCNT-S) composites in Figure 1a–d provided thorough information on the uniformity and size distribution of the active sulfur material. Compared with CNT-S, the uniform color and brightness of the OCNT-S indicates a homogeneous sulfur distribution. Another noticeable difference is that the sulfur loading on the CNT fiber results in big particles which may not contribute to the sulfur utilization. The diameter of such big particles is more than 10 µm. These differences could be attributed to the effect of oxygen functionalization that alters the surface energy of CNT and enhances the sulfur infusion and its uniform distribution. The oxygen functionalization of CNT was proven by XPS in our previous work [42]. The peaks for hydroxyl (C-OH), carbonyl (C = O), and carboxyl (-C = O-O-) were observed. The EDS analysis (Figure S1) proved the existence of sulfur in these CNT fiber composites. Further, the sulfur content distinctly varies at different spots on CNT-S, while it remains similar on OCNT-S. This is in line with the SEM observation. The EDS mapping (Figure S2) further confirmed the uniform distribution of elemental sulfur on the fiber.

Despite the difference in sulfur morphology, the TGA analysis (Figure 1g) revealed similar sulfur weight content of ~70% in these composites. The high sulfur content is crucial to increase the energy density of a Li-S battery if the high utilization of sulfur could also be achieved.

Another noticeable difference in Figure 1a,b is the diameter of the fibers, where the 83 µm diameter of OCNT-S fiber is shown to be greater than that of the CNT-S (70 µm). The

observed increase in diameter of OCNT-S could be attributed to the in-depth infusion of sulfur, which is confirmed by the X-ray CT images in Figure 1e,f. These images show a layer with light gray color which is likely because of sulfur infiltration. The depth of this layer is 20 μm, which is corresponds to half of the fiber radius. This result is in agreement with our previous findings on the oxygen plasma depth penetration [42], which further proves the correlation between the distribution of sulfur and oxygen plasma functionalization. The Brunauer–Emmett–Teller (BET) surface area of oxygen functionalized CNT was found to be 208.015 m^2/g, which is 23% higher than that of pristine CNT [42]. Although the high porosity of OCNT did not increase the sulfur loading much, it helped to load the sulfur deeper into the fiber which improved the utilization of sulfur active material.

In addition, Figure 1h shows the Raman spectra of CNT, OCNT, and OCNT-S samples, respectively. The I_D/I_G ratio of the samples increased after oxygen plasma functionalization, which could be attributed to the introduction of oxygen-based functional groups. Moreover, the in-depth sulfur loading in OCNT-S likely induced more defeats, resulting in an increased D peak. The OCNT-S also revealed three characteristic sulfur Raman peaks in the range of 100–600 cm^{-1} [21], indicating a successful integration of sulfur into OCNT. The results from the tensile strength test of pristine CNT fiber and after loading it with sulfur are displayed in Figure 1i. The tensile strength of the CNT fiber after loading with sulfur increased from 82 MPa to 102 MPa, which may be due to the consolidating effect of sulfur on the CNT bundles within the fiber.

The findings from these studies suggest that oxygen functionalization can influence the uniformity of sulfur distribution not only on the CNT fiber surface but also in its depth thus fully enhancing the sulfur utilization.

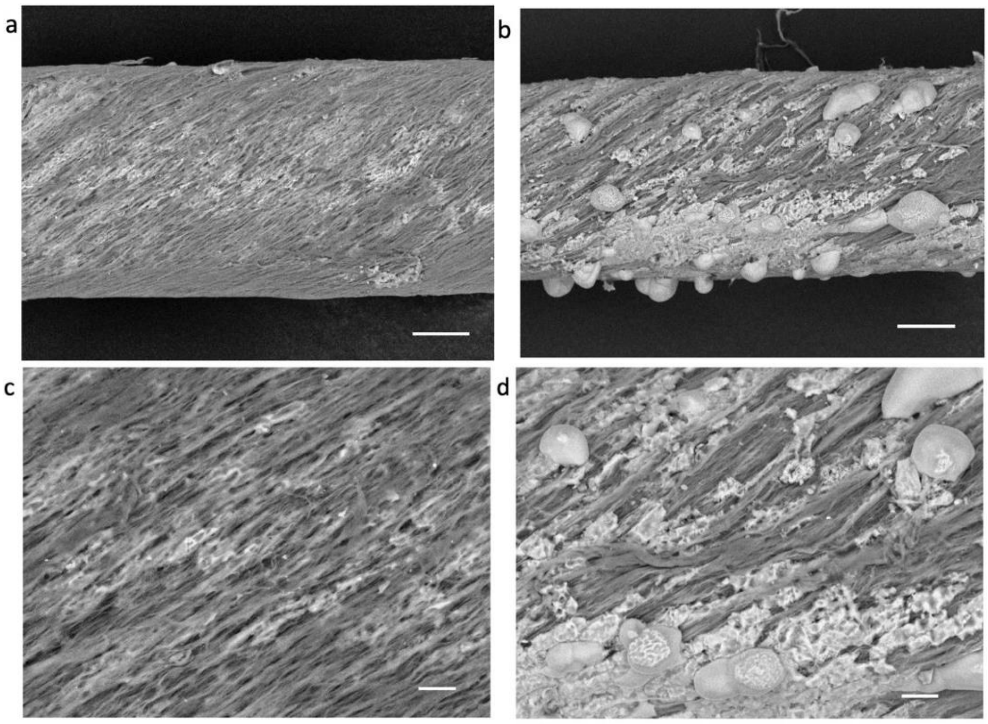

Figure 1. *Cont.*

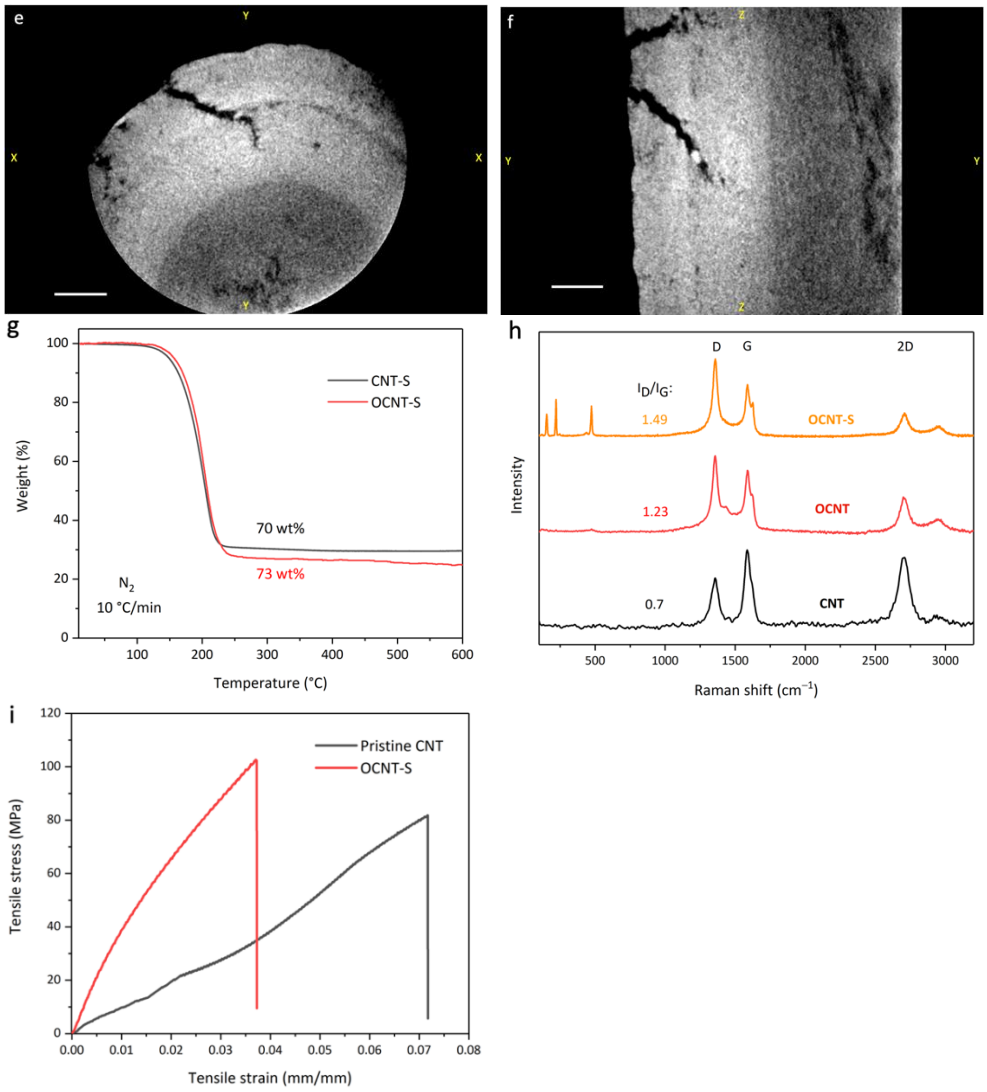

Figure 1. Low magnification SEM images of (**a**) OCNT-S, (**b**) CNT-S. High magnification SEM images of (**c**) OCNT-S, (**d**) CNT-S. The scale bars in the SEM images for (**a**,**b**) are 20 μm, and for (**c**,**d**) are 5 μm. (**e**) X-ray CT images of OCNT-S in XY slice. (**f**) X-ray CT images of OCNT-S in YZ slice. Scare bars for both (**e**,**f**) are 10 μm. (**g**) TGA curves for OCNT-S and CNT-S. (**h**) Raman spectra of CNT, OCNT, and OCNT-S, where characteristic peaks of sulfur were observed for CNT-S. The I_D/I_G ratios in all these samples are indicated. (**i**) Tensile stress vs. strain plot of pristine CNT and OCNT-S, respectively.

The electrochemical performance of CNT-S and OCNT-S fiber electrodes measured at different current densities (0.1 C to 2 C) is shown in Figure 2. The capacities were calculated based on the mass of sulfur in the composite fibers.

The rate performances of the CNT-S and OCNT-S were evaluated by increasing the charge/discharge current density stepwise from 0.1 C to 2 C every 5 cycles. As displayed in Figure 2a, when the cell is charged and discharged at 0.1 C, OCNT-S shows a discharge capacity of 1031 mAh g^{-1}. In Li-S energy storage system, the capacity decreases at a high current density due to increasing the polarization caused by insufficient ion transportation and high resistance of the electrode. At a higher rate of 0.5 C, the battery can still maintain a capacity of 580 mAh g^{-1}. Moreover, a capacity of approximately 800 mAh g^{-1}, about 78% of the original capacity, can be recovered when the current density is returned from 2 to 0.1 C. The flexibility and robustness of the fibrous electrode also contribute to the decent electrochemical performance under deformations. Compared with CNT-S, the capacity decays continuously from 938 to 671 mAh g^{-1} during the first 5 cycles at 0.1 C. A capacity

of 490 mAh g^{-1} was recovered when the cell was re-discharged at 0.1 C after a series of high rates tests, which is only 52% of the capacity of the first cycle. This is suggesting a loss of active materials after the cycling test due to deformation. In addition, the Coulombic efficiency of OCNT-S cells was much more stable and closer to 100% compared to CNT-S cells.

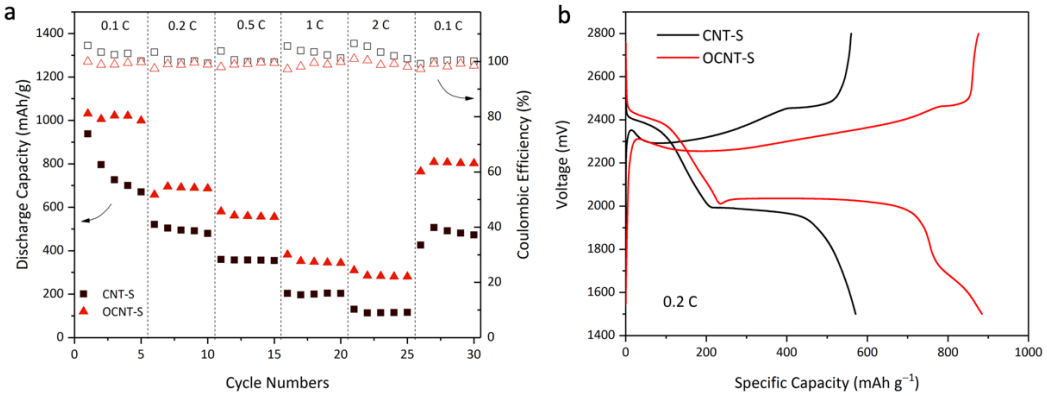

Figure 2. (**a**) Rate capability of Li-S cells with CNT-S and OCNT-S cathodes up to 2 C. (**b**) Discharge/charge profiles in the second cycle of Li-S cells with CNT-S and OCNT-S cathodes at a current density of 0.2 C.

The galvanostatic charge/discharge behavior of the CNT-S and OCNT-S was assessed at a current density of 0.2 C between 2.8 and 1.5 V versus Li/Li^+, as shown in Figure 2b. These two discharge profiles exhibit two plateaus typical for Li-S batteries, which correspond to the reduction of elemental sulfur (S_8) to long-chain LiPSs at 2.3–2.4 V along with the formation of short-chain Li_2S_2 and Li_2S at 2.0–2.1 V [43]. The OCNT-S exhibits a long voltage platform and small polarization compared to CNT-S, indicating a high utilization of sulfur and fast transportation of electrons and ions thanks to the oxygen functional groups, which exhibit a relatively high binding energy to polysulfide, as reported by others [18,20]. The short plateau near 1.7 V could be attributed to the discharge of sulfur loaded deeply inside the fiber. The plateau shifts due to less accessibility to the electrolyte.

Further, the cycling performance of CNT-S and OCNT-S cells was investigated at 0.1 C for up to 300 cycles. Figure 3a displays the long-term cycling performance of the two fibers at 0.1 C for 300 cycles. After 300 cycles, CNT-S delivered a capacity of 269 mAh g^{-1}, which is only 29.6% retention from the initial capacity of 909 mAh g^{-1}. In comparison, an initial capacity of 1019 mAh g^{-1} was delivered by OCNT-S cells and retained 474 mAh g^{-1} (near 47%) after running for 300 cycles. It was noted that especially for CNT-S, the capacity decay mainly took place within the first 30 cycles where the capacity of the cell was decreased by 38%. In the following 270 cycles, only a 32% decrease in capacity was observed. The capacity loss in the beginning may be attributed to the irreversible active material loss from the big sulfur particle caused by the electrode deformation, and by the free diffusion of polysulfides since oxygen functional groups were not present to trap them on the CNT fiber. Furthermore, the Coulombic efficiency of the OCNT-S cell was very stable after the first 10 cycles, with an average efficiency of 99.7% over the entire 300 cycles. Meanwhile, the Coulombic efficiency of the CNT-S cell was above 99% for the first 100 cycles, however, it gradually decreased below 99%, with an average efficiency of 98.9% over the complete 300 cycles. A possible explanation for the improvement in the OCNT-S cell is the effective polysulfide trapping due to the increased materials' porosity caused by the plasma functionalization [20,42] and the presence of oxygen functional groups.

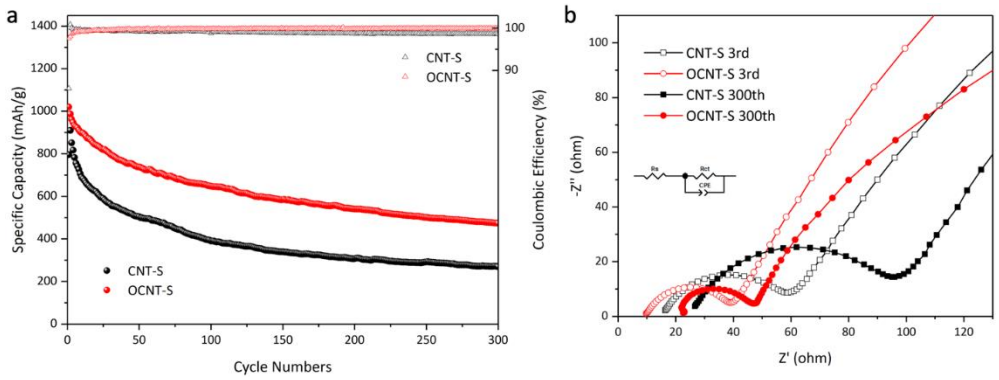

Figure 3. (**a**) Cycling performance of Li-S cells assembled with CNT-S and OCNT-S as cathodes at a current density of 0.1 C. (**b**) EIS spectra of the CNT-S and OCNT-S after 3 cycles and after 300 cycles.

Electrochemical impedance spectroscopy (EIS) was conducted after the first 3 cycles and after 300 cycles at 0.1 C, and the Nyquist plots of CNT-S and OCNT-S are displayed in Figure 3b. In general, the semicircle in the high-frequency region corresponds to the charge transfer resistance (R_{ct}) at the interface between the sulfur cathode and electrolyte. The internal resistance (R_s) is representing the electronic resistance of the cathode and the ionic resistance of the electrolyte [21]. In the early stage of the cyclic test, the OCNT-S electrode exhibits lower values of both R_s (9.8 vs. 16.4 Ω) and R_{ct} (29.5 vs. 43.6 Ω). A possible explanation for this difference is related to the CNT fiber electrode morphology and refined particle size of sulfur thanks to the presence of oxygen functional groups. After 300 cycles, OCNT-S reveals a small increase in R_s from 9.8 Ω to 22 Ω. Similarly, CNT-S shows an increase in R_s from 16.4 Ω to 26.7 Ω. The moderate rise in R_s could be a result of accumulating soluble polysulfides and deposition of insulating LiS on the electrodes during cycling, causing an increase in viscosity and resistance of the electrolyte and the electrode. Furthermore, the R_{ct} of CNT-S increased significantly after 300 cycles from 43.6 Ω to 69.5 Ω, which could be attributed to the free diffusion of polysulfide in the electrolyte along with deposition of insulating LiS on electrodes that decelerates the kinetics of the electrochemical reaction and raises the resistance. Meanwhile, OCNT-S reveals a slight decrease in R_{ct} from 29.5 Ω to 26.5 Ω. This reduction in the charge transfer resistance of OCNT-S could be a result of well-controlled polysulfide diffusion within the cathode which maintains the viscosity and ionic conductivity of the electrolyte. As a result, the formation of LiS on the anode due to polysulfides shuttling is suppressed. In addition, the redistribution of active materials on the cathode during cycling could improve the contact with the electrolyte. The described here outcomes revealed the positive effect of oxygen functional groups, created by plasma treatment of the CNT electrodes, in mitigating the diffusion of polysulfides from the cathode to the lithium anode thus enabling long-term stability of cycling.

4. Conclusions

We have demonstrated a freestanding and flexible CNT-S composite as a fiber-shaped electrode for Li-S batteries. The unique design of this electrode is featured by the oxygen plasma functionalization to accommodate a high content of sulfur, refine the sulfur particle size, and form uniform sulfur deposition. All these advantages benefit the batteries enabling effective utilization of the sulfur active material and mitigating the polysulfide shuttling effect. As a result, the OCNT-S electrode exhibits an improved rate capability and cycling stability. Particularly, the OCNT-S cathode, with a 73% high sulfur loading, retained 78% of the initial capacity at the originally applied current density of 0.1 C, after being cycled under various high current densities. In addition, the same cathode was able to deliver a capacity of 1019 mAh g^{-1} at 0.1 C loading and maintain 47% of the initial capacity after 300 cycles. We believe that the plasma-enhanced CNT fiber-cathode described and studied here is very promising for Li-S batteries which require lightweight, mechanical flexibility and the ability to be integrated into fabrics to support wearable electronic devices.

Supplementary Materials: The following supporting information can be downloaded at: https://www.mdpi.com/article/10.3390/c8020030/s1, Figure S1: EDS analysis of OCNT-S and CNT-S electrodes. (a1) Selected areas on the OCNT-S for analysis; (a2) EDS spectrum and element analysis data at different areas of OCNT-S; (b1) Selected areas on the CNT-S for analysis; (b2) EDS spectrum and element analysis data at different areas of CNT-S. Figure S2: (a) SEM image of OCNT-S, showing the selected area for EDS mapping. (b) Sulfur el-emental distribution of OCNT-S.

Author Contributions: Conceptualization, Y.F., Y.-Y.H. and V.S.; methodology, Y.F., Y.-Y.H. and S.N.K.; software, Y.F. and V.K.R.K.; validation, Y.F. and Y.-Y.H.; formal analysis, Y.F. and Y.-Y.H.; investigation, Y.F. and V.S.; resources, V.S.; data curation, Y.F., M.K., P.K.A., V.K.R.K. and B.S.; writing—original draft preparation, Y.F.; writing—review and editing, Y.F., Y.-Y.H., P.K.A., M.K. and V.S.; visualization, Y.F. and M.K.; supervision, V.S.; project administration, V.S.; funding acquisition, V.S. All authors have read and agreed to the published version of the manuscript.

Funding: This work was funded by NASA grants NNC16CA17C and 80NSSC21P2821, and by NSF grants CBET-1706489 and CBET-2028625.

Data Availability Statement: Data is available upon request.

Conflicts of Interest: The authors declare no conflict of interest.

References

1. Kim, J.; Lee, M.; Shim, H.J.; Ghaffari, R.; Cho, H.R.; Son, D.; Jung, Y.H.; Soh, M.; Choi, C.; Jung, S.; et al. Stretchable silicon nanoribbon electronics for skin prosthesis. *Nat. Commun.* **2014**, *5*, 5747. [CrossRef] [PubMed]
2. Melzer, M.; Kaltenbrunner, M.; Makarov, D.; Karnaushenko, D.; Karnaushenko, D.; Sekitani, T.; Someya, T.; Schmidt, O.G. Imperceptible magnetoelectronics. *Nat. Commun.* **2015**, *6*, 6080. [CrossRef] [PubMed]
3. Salvatore, G.A.; Münzenrieder, N.; Kinkeldei, T.; Petti, L.; Zysset, C.; Strebel, I.; Büthe, L.; Tröster, G. Wafer-scale design of lightweight and transparent electronics that wraps around hairs. *Nat. Commun.* **2014**, *5*, 2982. [CrossRef] [PubMed]
4. Li, L.; Wu, Z.; Yuan, S.; Zhang, X.-B. Advances and challenges for flexible energy storage and conversion devices and systems. *Energy Environ. Sci.* **2014**, *7*, 2101–2122. [CrossRef]
5. Hu, L.; La Mantia, F.; Wu, H.; Xie, X.; McDonough, J.; Pasta, M.; Cui, Y. Lithium-Ion Textile Batteries with Large Areal Mass Loading. *Adv. Energy Mater.* **2011**, *1*, 1012–1017. [CrossRef]
6. Hu, L.; Wu, H.; La Mantia, F.; Yang, Y.; Cui, Y. Thin, Flexible Secondary Li-Ion Paper Batteries. *ACS Nano* **2010**, *4*, 5843–5848. [CrossRef]
7. Dong, L.; Xu, C.; Li, Y.; Wu, C.; Jiang, B.; Yang, Q.; Zhou, E.; Kang, F.; Yang, Q.-H. Simultaneous Production of High-Performance Flexible Textile Electrodes and Fiber Electrodes for Wearable Energy Storage. *Adv. Mater.* **2016**, *28*, 1675–1681. [CrossRef]
8. Ji, H.; Zhang, L.; Pettes, M.T.; Li, H.; Chen, S.; Shi, L.; Piner, R.; Ruoff, R.S. Ultrathin Graphite Foam: A Three-Dimensional Conductive Network for Battery Electrodes. *Nano Lett.* **2012**, *12*, 2446–2451. [CrossRef]
9. Li, N.; Chen, Z.; Ren, W.; Li, F.; Cheng, H.-M. Flexible graphene-based lithium ion batteries with ultrafast charge and discharge rates. *Proc. Natl. Acad. Sci. USA* **2012**, *109*, 17360–17365. [CrossRef]
10. Zeng, W.; Shu, L.; Li, Q.; Chen, S.; Wang, F.; Tao, X. Fiber-based wearable electronics: A review of materials, fabrication, devices, and applications. *Adv. Mater.* **2014**, *26*, 5310–5336. [CrossRef]
11. Chen, X.; Lin, H.; Deng, J.; Zhang, Y.; Sun, X.; Chen, P.; Fang, X.; Zhang, Z.; Guan, G.; Peng, H. Electrochromic Fiber-Shaped Supercapacitors. *Adv. Mater.* **2014**, *26*, 8126–8132. [CrossRef] [PubMed]
12. Fang, X.; Yang, Z.; Qiu, L.; Sun, H.; Pan, S.; Deng, J.; Luo, Y.; Peng, H. Core-Sheath Carbon Nanostructured Fibers for Efficient Wire-Shaped Dye-Sensitized Solar Cells. *Adv. Mater.* **2014**, *26*, 1694–1698. [CrossRef] [PubMed]
13. Zhang, Y.; Bai, W.; Cheng, X.; Ren, J.; Weng, W.; Chen, P.; Fang, X.; Zhang, Z.; Peng, H. Flexible and Stretchable Lithium-Ion Batteries and Supercapacitors Based on Electrically Conducting Carbon Nanotube Fiber Springs. *Angew. Chem. Int. Ed.* **2014**, *53*, 14564–14568. [CrossRef] [PubMed]
14. Van Noorden, R. A better battery. *Nature* **2014**, *507*, 26. [CrossRef] [PubMed]
15. Zhu, J.; Ge, Y.; Kim, D.; Lu, Y.; Chen, C.; Jiang, M.; Zhang, X. A novel separator coated by carbon for achieving exceptional high performance lithium-sulfur batteries. *Nano Energy* **2016**, *20*, 176–184. [CrossRef]
16. Peng, H.; Wang, D.; Huang, J.; Cheng, X.-B.; Yuan, Z.; Wei, F.; Zhang, Q. Janus Separator of Polypropylene-Supported Cellular Graphene Framework for Sulfur Cathodes with High Utilization in Lithium–Sulfur Batteries. *Adv. Sci.* **2015**, *3*, 1500268. [CrossRef] [PubMed]
17. Hu, G.; Xu, C.; Sun, Z.; Wang, S.; Cheng, H.-M.; Li, F.; Ren, W. 3D Graphene-Foam-Reduced-Graphene-Oxide Hybrid Nested Hierarchical Networks for High-Performance Li-S Batteries. *Adv. Mater.* **2016**, *28*, 1603–1609. [CrossRef]
18. Shaibani, M.; Akbari, A.; Sheath, P.; Easton, C.; Banerjee, P.C.; Konstas, K.; Fakhfouri, A.; Barghamadi, M.; Musameh, M.M.; Best, A.S.; et al. Suppressed Polysulfide Crossover in Li–S Batteries through a High-Flux Graphene Oxide Membrane Supported on a Sulfur Cathode. *ACS Nano* **2016**, *10*, 7768–7779. [CrossRef]

19. Chung, S.-H.; Manthiram, A. Bifunctional Separator with a Light-Weight Carbon-Coating for Dynamically and Statically Stable Lithium-Sulfur Batteries. *Adv. Funct. Mater.* **2014**, *24*, 5299–5306. [CrossRef]
20. Hsieh, Y.-Y.; Zhang, L.; DeArmond, D.; Kanakaraj, S.N.; Adusei, P.K.; Alvarez, N.T.; Fang, Y.; Daum, J.; Shanov, V. Integrated graphene-sulfur cathode and separator with plasma enhancement for Li-S batteries. *Carbon N. Y.* **2018**, *139*, 1093–1103. [CrossRef]
21. He, J.; Chen, Y.; Li, P.; Fu, F.; Wang, Z.; Zhang, W. Three-dimensional CNT/graphene–sulfur hybrid sponges with high sulfur loading as superior-capacity cathodes for lithium–sulfur batteries. *J. Mater. Chem. A* **2015**, *3*, 18605–18610. [CrossRef]
22. Xiao, M.; Huang, M.; Zeng, S.; Han, D.; Wang, S.; Sun, L.; Meng, Y. Sulfur@graphene oxide core–shell particles as a rechargeable lithium–sulfur battery cathode material with high cycling stability and capacity. *RSC Adv.* **2013**, *3*, 4914–4916. [CrossRef]
23. Zheng, S.; Wen, Y.; Zhu, Y.; Han, Z.; Wang, J.; Yang, J.; Wang, C. In Situ Sulfur Reduction and Intercalation of Graphite Oxides for Li-S Battery Cathodes. *Adv. Energy Mater.* **2014**, *4*, 1400482. [CrossRef]
24. Xiao, Z.; Yang, Z.; Nie, H.; Lu, Y.; Yang, K.; Huang, S. Porous carbon nanotubes etched by water steam for high-rate large-capacity lithium–sulfur batteries. *J. Mater. Chem. A* **2014**, *2*, 8683–8689. [CrossRef]
25. Chen, J.-J.; Zhang, Q.; Shi, Y.-N.; Qin, L.-L.; Cao, Y.; Zheng, M.-S.; Dong, Q.-F. A hierarchical architecture S/MWCNT nanomicrosphere with large pores for lithium sulfur batteries. *Phys. Chem. Chem. Phys.* **2012**, *14*, 5376–5382. [CrossRef]
26. Xu, J.; Shui, J.; Wang, J.; Wang, M.; Liu, H.; Dou, S.X.; Jeon, I. Sulfur–Graphene Nanostructured Cathodes *via* Ball-Milling for High-Performance Lithium–Sulfur Batteries. *ACS Nano* **2014**, *8*, 10920–10930. [CrossRef]
27. Wang, H.; Yang, Y.; Liang, Y.; Robinson, J.T.; Li, Y.; Jackson, A.; Cui, Y.; Dai, H. Graphene-Wrapped Sulfur Particles as a Rechargeable Lithium–Sulfur Battery Cathode Material with High Capacity and Cycling Stability. *Nano Lett.* **2011**, *11*, 2644–2647. [CrossRef]
28. Wang, J.-Z.; Lu, L.; Choucair, M.; Stride, J.A.; Xu, X.; Liu, H.-K. Sulfur-graphene composite for rechargeable lithium batteries. *J. Power Sources* **2011**, *196*, 7030–7034. [CrossRef]
29. Xu, C.; Wu, Y.; Zhao, X.; Wang, X.; Du, G.; Zhang, J.; Tu, J. Sulfur/three-dimensional graphene composite for high performance lithium–sulfur batteries. *J. Power Sources* **2015**, *275*, 22–25. [CrossRef]
30. Zhou, G.; Yin, L.-C.; Wang, D.-W.; Li, L.; Pei, S.; Gentle, I.R.; Li, F.; Cheng, H.-M. Fibrous Hybrid of Graphene and Sulfur Nanocrystals for High-Performance Lithium–Sulfur Batteries. *ACS Nano* **2013**, *7*, 5367–5375. [CrossRef]
31. Peng, H.-J.; Huang, J.-Q.; Zhao, M.-Q.; Zhang, Q.; Cheng, X.-B.; Liu, X.-Y.; Qian, W.-Z.; Wei, F. Nanoarchitectured Graphene/CNT@Porous Carbon with Extraordinary Electrical Conductivity and Interconnected Micro/Mesopores for Lithium-Sulfur Batteries. *Adv. Funct. Mater.* **2014**, *24*, 2772–2781. [CrossRef]
32. Lin, H.; Weng, W.; Ren, J.; Qiu, L.; Zhang, Z.; Chen, P.; Chen, X.; Deng, J.; Wang, Y.; Peng, H. Twisted Aligned Carbon Nanotube/Silicon Composite Fiber Anode for Flexible Wire-Shaped Lithium-Ion Battery. *Adv. Mater.* **2014**, *26*, 1217–1222. [CrossRef] [PubMed]
33. Ren, J.; Zhang, Y.; Bai, W.; Chen, X.; Zhang, Z.; Fang, X.; Weng, W.; Wang, Y.; Peng, H. Elastic and Wearable Wire-Shaped Lithium-Ion Battery with High Electrochemical Performance. *Angew. Chem. Int. Ed.* **2014**, *53*, 7864–7869. [CrossRef] [PubMed]
34. Weng, W.; Sun, Q.; Zhang, Y.; Lin, H.; Ren, J.; Lu, X.; Wang, M.; Peng, H. Winding Aligned Carbon Nanotube Composite Yarns into Coaxial Fiber Full Batteries with High Performances. *Nano Lett.* **2014**, *14*, 3432–3438. [CrossRef]
35. Xu, P.; Wei, B.; Cao, Z.; Zheng, J.; Gong, K.; Li, F.; Yu, J.; Li, Q.; Lu, W.; Byun, J.-H.; et al. Stretchable Wire-Shaped Asymmetric Supercapacitors Based on Pristine and MnO_2 Coated Carbon Nanotube Fibers. *ACS Nano* **2015**, *9*, 6088–6096. [CrossRef]
36. Chong, W.G.; Huang, J.-Q.; Xu, Z.-L.; Qin, X.; Wang, X.; Kim, J.-K. Lithium-Sulfur Battery Cable Made from Ultralight, Flexible Graphene/Carbon Nanotube/Sulfur Composite Fibers. *Adv. Funct. Mater.* **2017**, *27*, 1604815. [CrossRef]
37. Fang, X.; Weng, W.; Ren, J.; Peng, H. A Cable-Shaped Lithium Sulfur Battery. *Adv. Mater.* **2016**, *28*, 491–496. [CrossRef]
38. Huang, J.-Q.; Zhuang, T.-Z.; Zhang, Q.; Peng, H.-J.; Chen, C.-M.; Wei, F. Permselective Graphene Oxide Membrane for Highly Stable and Anti-Self-Discharge Lithium–Sulfur Batteries. *ACS Nano* **2015**, *9*, 3002–3011. [CrossRef]
39. Kanakaraj, S.N.; Alvarez, N.T.; Gbordzoe, S.; Lucas, M.S.; Maruyama, B.; Noga, R.; Hsieh, Y.-Y.; Shanov, V. Improved dry spinning process at elevated temperatures for making uniform and high strength CNT fibers. *Mater. Res. Express* **2018**, *5*, 065036. [CrossRef]
40. Kang, W.; Deng, N.; Ju, J.; Li, Q.; Wu, D.; Ma, X.; Li, L.; Naebe, M.; Cheng, B. A review of recent developments in rechargeable lithium–sulfur batteries. *Nanoscale* **2016**, *8*, 16541–16588. [CrossRef]
41. Xu, G.; Ding, B.; Pan, J.; Nie, P.; Shen, L.; Zhang, X. High performance lithium–sulfur batteries: Advances and challenges. *J. Mater. Chem. A* **2014**, *2*, 12662–12676. [CrossRef]
42. Adusei, P.K.; Gbordzoe, S.; Kanakaraj, S.N.; Hsieh, Y.-Y.; Alvarez, N.T.; Fang, Y.; Johnson, K.; McConnell, C.; Shanov, V. Fabrication and study of supercapacitor electrodes based on oxygen plasma functionalized carbon nanotube fibers. *J. Energy Chem.* **2020**, *40*, 120–131. [CrossRef]
43. Zhou, G.; Li, L.; Wang, D.-W.; Shan, X.-Y.; Pei, S.; Li, F.; Cheng, H.-M. A Flexible Sulfur-Graphene-Polypropylene Separator Integrated Electrode for Advanced Li-S Batteries. *Adv. Mater.* **2015**, *27*, 641–647. [CrossRef] [PubMed]